JVI
Journals.ASM.org

Mutations at the Base of the Icosahedral Five-Fold Cylinders of Minute Virus of Mice Induce 3′-to-5′ Genome Uncoating and Critically Impair Entry Functions

Susan F. Cotmore[a] and Peter Tattersall[a,b]

Departments of Laboratory Medicine[a]; and Genetics,[b] Yale University School of Medicine, New Haven, Connecticut, USA

The linear single-stranded DNA genome of minute virus of mice can be ejected, in a 3′-to-5′ direction, via a cation-linked uncoating reaction that leaves the 5′ end of the DNA firmly complexed with its otherwise intact protein capsid. Here we compare the phenotypes of four mutants, L172T, V40A, N149A, and N170A, which perturb the base of cylinders surrounding the icosahedral 5-fold axes of the virus, and show that these structures are strongly implicated in 3′-to-5′ release. Although noninfectious at 37°C, all mutants were viable at 32°C, showed a temperature-sensitive cell entry defect, and, after proteolysis of externalized VP2 N termini, were unable to protect the VP1 domain, which is essential for bilayer penetration. Mutant virus yields from multiple-round infections were low and were characterized by the accumulation of virions containing subgenomic DNAs of specific sizes. In V40A, these derived exclusively from the 5′ end of the genome, indicative of 3′-to-5′ uncoating, while L172T, the most impaired mutant, had long subgenomic DNAs originating from both termini, suggesting additional packaging portal defects. Compared to the wild type, genome release *in vitro* following cation depletion was enhanced for all mutants, while only L172T released DNA, in both directions, without cation depletion following proteolysis at 37°C. Analysis of progeny from single-round infections showed that uncoating did not occur during virion assembly, release, or extraction. However, unlike the wild type, the V40A mutant extensively uncoated during cell entry, indicating that the V40-L172 interaction restrains an uncoating trigger mechanism within the endosomal compartment.

The parvovirus minute virus of mice (MVM) has a 5-kb linear single-stranded, negative-sense DNA genome that is packaged vectorially, in a 3′-to-5′ direction, into small (~280-Å diameter) preassembled nonenveloped protein capsids, probably driven by the viral helicase, NS1 (9, 19). However, this genome can also be ejected from the otherwise intact infectious virion at physiological temperatures, again in a 3′-to-5′ direction, by divalent cation depletion, in a process that leaves the 5′ end of the genome firmly complexed with the particle (7). Similarly, it has been shown that during the final stages of desiccation, MVM ejects its genome from the capsid, which nevertheless remains intact, resisting collapse or disintegration (4). These observations raise the possibility that the exceptionally robust MVM particle may have specifically evolved to expose the 3′ end of its genome *in vivo* in response to a physiological stimulus, undergoing a conformational shift that leaves the uncoated DNA associated with the intact capsid, which might then play additional roles in the viral life cycle. In this study, we probed potential exit routes for this reaction by examining a group of capsid mutants, one of which, L172T, we have previously shown has a temperature-sensitive cell entry defect and can be induced to expose its DNA *in vitro* by proteolytic cleavage of the N terminus of its major capsid protein, VP2, at 37°C (11).

MVM expresses two forms of capsid protein, VP1 and VP2, which encode the same C-terminal 587 amino acids but are translated from differentially spliced mRNA to generate VP1 molecules with an additional 142-amino-acid N terminus-specific region denoted VP1SR (24). In the X-ray crystal structure, the MVM capsid shell is seen to comprise 549 amino acids from the common VP C termini, leaving N-terminal extensions of 38 residues from VP2 and 180 residues from VP1 that resist icosahedral averaging (1, 21). Sixty VP polypeptides, at a VP1/VP2 ratio of about 1:5 (29), preassemble *in vivo* into empty particles that appear structurally very similar to full virions in X-ray reconstructions (1, 20) but in which the N-terminal peptides are all internalized, making them inaccessible to exogenous proteases and antibodies (6, 30). However, because both VP1 and VP2 N termini carry protein motifs that are required for specific steps in host cell trafficking, they become sequentially exposed at the surface of the intact virion during maturation and host cell penetration (10). Thus, although the parvovirus capsid is exceptionally tough, it is also metastable, undergoing a program of limited rearrangements that begin, concomitant with early stages in DNA encapsidation, with the surface exposure of ~25 amino acids from the N termini of a subset of VP2 molecules (9). Mature virions are released from parental cells with this first wave of exposed N termini intact (6), but they are highly susceptible to proteolysis in the extracellular environment and during attachment and entry into host cells. Remarkably, such cleavage appears to allow the truncated terminus to be retracted (16) and replaced with an intact N terminus, so that ultimately around 90% of the ~50 VP2 termini become surface exposed and cleaved, giving rise to a third form of the capsid protein, VP3 (30).

Cylindrical projections encircled by conserved canyon-like depressions of undefined function surround each icosahedral 5-fold axis in the capsid shell. The outer part of these cylinders, formed by juxtaposition of antiparallel β-ribbons from the five symmetry-related VPs, is linked to a multilayered funnel-like base, and both

Received 23 August 2011 Accepted 11 October 2011
Published ahead of print 19 October 2011
Address correspondence to Peter Tattersall, peter.tattersall@yale.edu.

doi:10.1128/JVI.06119-11

enclose a narrow central channel that runs from the interior of the capsid to its outer surface. Despite their apparently minimal diameter, structural evidence implicates these pores as the routes of VP2 N-terminal egress and suggests that one of them serves as the entry portal for viral DNA (1, 25). However, to date only one residue, L172, which lines the pore at the base of the β-ribbon cylinder, creating its tightest (8-Å) internal constriction, has been examined in detail by mutagenesis (11, 12). With the exception of two viable mutants (L172I and L172V), all other amino acid substitutions introduced at this position in the immunosuppressive MVM variant (MVMi) proved noninfectious for various reasons, including failure to assemble capsids, package DNA, or initiate infection (12). However, unlike MVMi, wild-type virus from the prototype MVM strain (MVMp) can be cultured at 32°C, and in this background L172T was found to be temperature sensitive, being viable at 32°C but not at 37°C, due to a protracted cell entry defect(s) that continued for up to 8 h after particles were internalized. In this study, we compared the phenotypes of L172T and three additional mutants, N149A, N170A, and V40A, which were previously shown to be noninfectious at 37°C in human 324K cells (26). Virus-like particles (VLPs) generated from these mutants gave atypical tryptophan fluorescence emission shifts upon incremental heating, indicating a possible defect in capsid dynamics (26). We show here that, like L172T, these mutants are temperature sensitive and exhibit significant cell entry defects at 37°C. In particular, we have focused on V40A because this valine is positioned at the base of the cylinder immediately next to the glycine-rich sequence that changes position when VP N termini are extruded to the particle surface or when externalized VP2 N termini are cleaved and retracted. In X-ray structures of wild-type MVM, the hydrophobic side chains of V40 and L172 interact, and recent data suggest that this contact is critical for stabilizing interactions between the cylinder and the VP N termini (25). Thus, when tryptophan was substituted for leucine at L172, disrupting the V40 interaction, VP residues 39 to 45 became disordered and the N termini were displaced, allowing formation of an intense spherical density adjacent to W172 that effectively blocked the pore and prevented DNA encapsidation (25). This suggests that the primary function of the valine 40 side chain is to position and stabilize the VP termini at the base of the pore, whereas L172 plays a more complex role in pore dynamics, since 5-fold-related copies of its side chain also dictate pore diameter and character at its tightest constriction point at the cylinder base. The V40A mutant thus allows us to compare the effects of disrupting just the leucine-valine side chain interaction with the more complex L172T phenotype. We find that the ability of all of these mutants to protect their VP1 N termini is critically dependent upon the presence of intact VP2 N termini and that they readily expose their genomes, in a 3′-to-5′ direction, both *in vitro* following divalent cation depletion and *in vivo* during cell entry, implicating the cylinders as the likely route of genome egress during the 3′-to-5′ uncoating reaction. Additionally, the L172T mutant is prone to release its genome in a 5′-to-3′ direction after VP2 cleavage at 37°C, suggesting that this mutation also severely compromises the packaging portal, making it unable to retain the 5′ end of the packaged strand.

MATERIALS AND METHODS

Cells and viruses. The fibrotropic prototype strain of MVM (MVMp, GenBank accession number J02275) was grown in monolayer cultures of A9 ouabr11 cells in Dulbecco's modified Eagle's medium (DMEM) containing 5% fetal bovine serum (FBS) and antibiotics. A mutant carrying a leucine-to-threonine substitution at position 172 in the VP2 sequence (L172T, CT-to-AC mutation at MVM nucleotides [nt] 3308 and 3309) has been described previously (11). Alanine substitutions at VP2 positions N149 (AA-to-GC mutation at MVM nt 3239 and 3240), N170 (AA-to-GC substitution at nt 3302 and 3303), and V40 (T-to-C mutation at nt 2913) in pMVMp, an infectious plasmid clone of MVMp (15), were the kind gift of Mauricio Mateu (26).

Transfection-based virus expansion assays and generation of virus stocks. The viruses' ability to productively infect A9 cells was determined using a transfection-based virus expansion assay in which transfected A9 cells, seeded on Teflon-coated spot slides at 20% confluence, were cultured in the presence or absence of 1% neutralizing polyclonal anti-MVM capsid antibody for 2 days at 37°C or 3 days at 32°C. Cells were fixed, permeabilized, and stained for NS1 by indirect immunofluorescence, using the murine monoclonal antibody CE10B10 (32). Nuclei were counterstained with 4′,6-diamidino-2-phenylindole (DAPI), and the percentages of cells with NS1-positive nuclei were scored using a Zeiss Axio Imager M2 fluorescence microscope.

To generate virus stocks, A9 monolayers were transfected and cultured overnight at 37°C. The next day, cells from each 60-mm plate were distributed among three 100-mm plates, which were then incubated at 37°C or 32°C until cytopathic effects appeared or until cells reached confluence. Cells were washed in cold phosphate-buffered saline (PBS) containing complete EDTA-free protease inhibitor cocktail (PIC; Roche), scraped into the same buffer, and pelleted before being resuspended in either 0.5 ml 50 mM Tris-HCl–0.5 mM EDTA (pH 8.7) (TE8.7) per 100-mm plate and immediately frozen or being resuspended in 0.4 ml of cold 50 mM Tris-HCl (pH 8.0) containing PIC and lysed by mixing with 0.1 ml of the same buffer containing 1% SDS before being rapidly frozen and stored at −20°C. Virus was extracted from the TE8.7 pellets by repeated (three times) freezing and thawing at room temperature and from Tris-SDS pellets by thawing once, both extracts were clarified by centrifugation at 15,000 × *g* for 30 min at 4°C, and 5-ml amounts were fractionated on preparative iodixanol step gradients as previously described (7).

Analysis of capsid proteins. Samples were separated by SDS-PAGE using 7.5% acrylamide-0.2% bisacrylamide gels, and proteins were electroblotted onto polyvinylidene difluoride membranes. These were blocked, incubated with rabbit antibody against the "allo-p" peptide spanning amino acids 311 to 327 in MVMp VP2 (which was combined, as indicated for some analyses, with antibody directed against 141 amino acids of the VPSR; both antibodies are described in reference 6), and developed using an ECL system (Amersham, Uppsala, Sweden). Where indicated, virus particles in PBS were digested, as indicated, with tosylsulfonyl phenylalanyl chloromethyl ketone (TPCK)-trypsin, *Nα-p*-tosyl-*l*-lysine chloromethyl ketone (TLCK)-chymotrypsin, or proteinase K at a 2-ng/μl final concentration, and the reactions were stopped by adding EDTA to 20 mM and boiling in Laemmli sample buffer. When the infectivity of samples was to be examined after digestion, trypsin was inactivated by dilution in DMEM containing 10% FBS.

Analysis of viral DNA by Southern transfer and differential hybridization. Encapsidated DNA was quantified, before or after digestion with micrococcal nuclease as indicated, by denaturing agarose gel electrophoresis and Southern blotting. Membranes were hybridized using ^{32}P-labeled, random-primed probes that represented either the full-length MVM genome or ~200-bp PCR products derived from specific regions, as follows: MVM nt 789 to 1043 (1-kb probe), 1818 to 2106 (2-kb probe), 2849 to 3120 (3-kb probe), or 3976 to 4154 (4-kb probe). Alternatively, as indicated, hybridization probes were ^{32}P-5′-gamma-labeled positive-sense oligonucleotides representing MVM nt 207 to 233 (0.2-kb probe), 1985 to 2014 (2-kb probe), 2199 to 2228 (2.2-kb probe), 2872 to 2897 (2.9-kb probe), 4808 to 4832 (4.8-kb probe), or 4850 to 4874 (4.9-kb probe). DNA was quantified using a Typhoon Trio variable-mode imager (GE Healthcare) and ImageQuant TL 7.0 image analysis software (GE Healthcare).

Infectivity assays. To assess the ability of viruses to initiate infection, 25% confluent monolayers of A9 cells growing on spot slides were infected at various genome equivalents per cell in DMEM containing 1% FBS and

25 mM HEPES, pH 7.0. Infections were carried out for 4 to 8 h at either 32°C or 37°C, as indicated. After infection, cultures were incubated at the appropriate temperature in DMEM containing 5% FBS and *Clostridium perfringens* neuraminidase (Sigma-Aldrich, St. Louis, MO) added at 0.1 mg/ml to prevent reinfection. Cells were fixed at 26 h postinfection and stained and scored for NS1 expression as described above.

***In vitro* analysis of uncoating.** To analyze the effects of heat or proteolysis in the absence of divalent cation depletion, virus samples (typically ~1.2×10^{10} purified wild-type or mutant virions in 60 μl of 45% iodixanol buffered with PBS containing 5mM KCl and 1 mM $HgCl_2$ [KM]) were diluted to 300 μl with PBS in microcentrifuge tubes that had been precoated with 10 mg/ml bovine serum albumin (BSA). Samples were heated and/or digested with TPCK-trypsin at 2 ng/μl in the presence of 5 μM $CaCl_2$ for 1 h, as indicated. After addition of defined trypsin inhibitor (Cascade Biologics, Portland, OR) to 10 times the predicted effective dose, samples were diluted to 1 ml with PBS containing 0.5 mM EDTA and layered on top of 4 ml analytical iodixanol step gradients, comprising 0.75 ml of 55%, 1.5 ml of 45%, 1 ml of 35%, and 0.75 ml of 15% iodixanol in PBS-KM. Gradients were centrifuged at 40,000 rpm for 18 h at 18°C in a Beckman SW50.1 rotor, and fractions were collected from the bottom as described above. All gradient tubes were precoated with BSA or 1% low-IgG fetal bovine serum in PBS to minimize virus loss.

To analyze the effects of divalent cation depletion, similar virus samples in 45% iodixanol–PBS-KM were diluted into 3 volumes of TE8.7 in BSA-coated tubes and stored at 4°C for the times indicated. Samples were then diluted to 300 μl in 50 mM Tris-HCl (pH 7.5), heated and/or digested as specified, and processed and fractionated as described above.

Analysis of DNA replication in single-round infections. A9 cell monolayers at 50% confluence in 60-mm dishes were infected with virions from fraction 5 of the wild-type and mutant gradients (see Fig. 2) at 10,000 genomes/cell in DMEM containing 1% FBS and incubated at 32°C or 37°C. Neuraminidase was added to cultures to remove surface virus from cells and prevent reinfection, and cells and medium from the 37°C and 32°C cultures were harvested at 26 h and 31 h postinfection, respectively. Cells were recovered by trypsinization, washed twice with PBS containing protease inhibitors, divided into two aliquots, and pelleted by centrifugation.

Cells from one half of the plate were resuspended in 0.1 ml of TE8.7 and flash frozen. These were frozen and thawed three times to release virus, and the resulting supernatants were analyzed before and after micrococcal nuclease treatment on denaturing gels by Southern blotting to look for encapsidated subgenomic DNAs. Samples of the recovered tissue culture medium were similarly analyzed before and after digestion with nuclease.

Cells from the second half of each plate were resuspended in 0.1 ml of 10 mM Tris-HCl (pH 7.5) containing 10 mM NaCl and 4% NP-40 and flash frozen for analysis of total viral DNA. These samples were later extracted by mixing with 50 mM Tris-HCl, 20 mM EDTA, and 2% SDS at room temperature and adjusted to a total volume of 400 μl containing 50 mM Tris-HCl, 15 mM EDTA, 0.5% SDS, 1% NP-40, and 200 mM NaCl before addition of 100 μg proteinase K and incubation at 45°C for 2 h and 60°C for 30 min and cooling to room temperature overnight. Total DNA from aliquots of these digests (100 μl) was then prepared using QIAquick PCR purification units (Qiagen) and analyzed by electrophoresis through neutral agarose gels and Southern transfer.

Cell entry assays. Cells were synchronized and prevented from entering S phase using a double-block procedure described previously (8). Briefly, 25% confluent A9 monolayers were allowed to accumulate in G_0 by withholding isoleucine for 40 h at 37°C, then transferred to medium containing the DNA polymerase inhibitor aphidicolin at 10 μg/ml together with MVM wild-type or V40A virions (50,000 genomes/cell), and incubated at 32°C for 24 h before neuraminidase was added to release all noninternalized virus from the cell surface. Cells and medium were harvested at 28 h postinfection.

At harvest, cells were washed with ice-cold PBS containing PIC, scraped into this buffer, and pelleted by centrifugation. After addition of 0.4 ml Tris-HCl (pH 8.0) containing PIC and 1 mM EDTA, uninfected control cells received 1/10 of the V40A inoculum used to infect the test plate in order to monitor any virus disruption that might occur during the extraction procedure. Cells then received 0.1 ml of the same buffer containing 1% SDS, and samples were briefly mixed and flash frozen. Samples were fractionated through a preparative iodixanol gradient as described above to generate virus stocks and analyzed before and after nuclease treatment by Southern blotting.

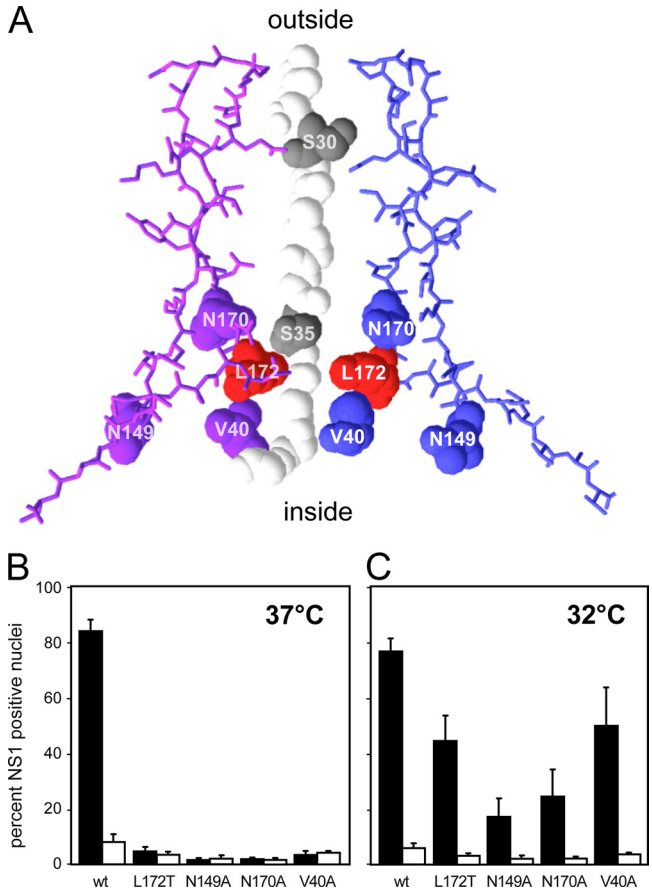

FIG 1 Mutations at the base of the 5-fold cylinder make MVMp virions temperature sensitive for growth. (A) Molecular model, made using Deep View Swiss PDB viewer and PDB 1MVM, depicting a cross-section of a single 5-fold cylinder. Amino acid residues from two of the five VP subunits that form the cylinder walls are represented as stick diagrams. Residues L172, N149, N170, and V40, which were mutated for this study, are highlighted as space-filling renditions. A space-filling rendition of a single glycine-rich VP2 sequence is modeled traversing the pore. This comprises a string of 10 glycine residues, between positions 28 and 39, interrupted by two serine residues at positions 30 and 35, as indicated. (B and C) Virus expansion assays in A9 cells transfected with wild-type (wt) or mutant MVMp-based infectious clones, cultured in the presence (black bars) or absence (white bars) of a neutralizing anticapsid antibody at either 37°C (B) or 32°C (C) and stained for NS1 on days 3 or 4 after transfection, respectively. Experiments were performed in duplicate, with each data point representing between 500 and 1,000 cells.

RESULTS

MVMp VP2 mutants N170A, N149A, and V40A are temperature sensitive. MVMp genomes with alanine mutations near the base of the 5-fold cylinders at positions N149, N170, and V40 in the VP2 capsid gene (Fig. 1A) were reported to be nonviable following transfection into 324K cells at 37°C (26). To compare the effects of these mutations with that of L172T, we first used virus expansion assays in which infectious plasmid clones were transfected into A9

cells, which were then either cultured alone or in the presence of neutralizing anticapsid antibody on multispot microscope slides at 37°C or 32°C. At 37°C wild-type virus expanded through the cultures by day 3 posttransfection, as assessed by immunofluorescent staining for the viral NS1 protein, infecting >80% of cells via a route that was sensitive to antibody-mediated neutralization. However, none of the mutants were able to spread through the culture, irrespective of the presence or absence of antibody (Fig. 1B). In contrast, at 32°C all of the viruses showed antibody-sensitive expansion (Fig. 1C), although each of the mutants was impaired relative to wild-type virus. Since these viruses spread effectively at the lower temperature, the N149A, L170A, and V40A mutations do not render the 5-fold cylinder of the virus inflexible and hence unable to support structural shifts that are needed during virus entry, as initially supposed. Instead, this indicates that, as in L172T, at normal physiological temperatures the cylinders of these mutants are compromised.

To further explore this phenotype and to derive virus stocks, we again transfected A9 cells with wild-type and mutant genomes and divided the resulting cells between multiple plates, which were cultured at 37°C or 32°C and monitored for evidence of virus-mediated cytotoxicity. At 37°C, wild-type genomes induced cytotoxicity leading to widespread cell lysis by day 3 posttransfection, whereas cells receiving mutant genomes continued to expand in parallel with uninfected controls until they reached confluence on day 6 posttransfection, when they were harvested and shown to lack conspicuous virus capsid accumulation as assessed by a hemagglutination assay (not shown). In contrast, cells transfected with wild-type genomes and cultured at 32°C showed extensive lysis by day 4 posttransfection, while those receiving mutant genomes survived for 6 to 7 days posttransfection before succumbing in a similar manner. Extracts prepared from such cultures had hemagglutinating activity (not shown), indicating that assembled capsid particles were present and thus confirming that all of the mutant viruses were able to amplify through the culture at 32°C, albeit somewhat less efficiently than wild-type virus.

Mutants produce low virion yields and accumulate atypical particles. We have previously shown that protracted exposure to the standard cell extraction buffer, TE8.7, followed by incubation at 37°C induces a novel genome rearrangement in wild-type virus that we term cation-linked uncoating (7). To avoid the possibility of such *in vitro* modification in this study and to ensure the quantitative extraction of virus from cells, the samples illustrated in Fig. 2 were derived by lysing cell pellets with 0.2% SDS on ice at pH 8.0, as described in Materials and Methods. As expected, capsid proteins in the wild-type extract (Fig. 2A) migrated as two major peaks, one of full infectious virions banding in fractions 4 to 6 and a more abundant peak of empty particles in fractions 10 to 13. As seen in the left panels of Fig. 2B through E, the gradient profiles for each mutant were very different from that for the wild type but were similar to each other in the following ways: (i) in each case the peak of full particles in fractions 4 to 6 was diminished, ranging from ~2 to 13% of the wild-type yield; (ii) capsid proteins were more widely dispersed through the gradients, showing substantial accumulation in fractions 7 to 9, which normally contain few wild-type particles; and (iii) these atypical accumulations all contained VP3. Since VP3 is usually generated during entry by proteolytic cleavage of VP2 N termini, which are exposed only in full virions, this suggests that the mutant particles with atypical sedimentation rates likely were, or had been, packaged with some form of the viral DNA. It also suggests that the accumulated intracellular particles had been subjected to extensive proteolysis, which presumably could have occurred at several points in their history, including during cell entry, progeny virus production, or cell extraction.

To explore these structures in more detail, we subjected various fractions to proteolysis *in vitro* at 37°C using trypsin, chymotrypsin, and proteinase K. Following such treatment, V40A mutant empty particles from fraction 11 and empty control particles from fraction 11 of the wild-type gradient showed no evidence of further cleavage (not shown), indicating that mutant empty particles, like their wild-type counterparts, do not have exposed VP2 N termini that could be cleaved to generate the VP3 forms seen dispersed throughout the gradients. Similarly, fraction 9 samples from the mutant gradients, which contained both VP2 and VP3 forms, were not further cleaved by these enzymes (not shown). This suggests that fraction 9 might contain a mixture of two types of particles, one representing partially packaged or partially uncoated virions in which VP2 has mostly been cleaved to VP3 and the other representing some form of dense VP2-only empty particle, although other explanations are possible. We conclude that these mutant particles do not exhibit abnormal protease cleavage patterns and that the VP3 forms distributed throughout the mutant gradients are derived from virions and not from empty particles. The gradient profiles thus suggest that the low virion yields seen in fractions 4 to 6 reflect, at least in part, the decreased stability of mutant virions.

Protected subgenomic DNA species are derived from partially uncoated virions. The right-hand panels in Fig. 2 show encapsidated DNA in these gradient fractions, detected by Southern blotting with a full-length genomic probe following micrococcal nuclease digestion and electrophoresis through denaturing gels. Most of the DNA in gradients of wild-type virus was ~5 kb in length and occurred in fractions 4 to 6. In the gradients of mutant virions, the limited number of protected 5-kb genomes were again mostly confined to fractions 4 to 6, but these corresponded to only 2% to 9% of the wild-type yield. However, there were also many subgenomic forms that fractionated through the gradient, correlating with the atypical distribution of VP3-containing particles seen in the Western blots in Fig. 2.

The subgenomic DNA fragments observed in fractions 5 to 8 of the mutant gradients showed a characteristic size distribution, with specific major size classes of ~2.3 to 3.5 kb. We have previously reported a similar pattern of subgenomic forms in wild-type particles following incomplete cation-linked uncoating reactions (7). To determine the origin of the subgenomic sequences produced by these mutants, we probed fractions 4 to 8 from the V40A gradient with labeled oligonucleotides derived from various positions along the genome (Fig. 3A). While sequences from the left (3′) end of the negative-sense strand (MVM nt 207 to 233) hybridized predominantly with full-length genomes, those positioned nearer the right end also detected progressively smaller subgenomic species. These included a somewhat heterogeneous smear of long fragments (3.5 to 5 kb) in fraction 5 and a cluster of major discrete bands in fractions 6 to 8, labeled a, b, and c in Fig. 3A, against a background of more heterogeneous forms. Of the major species, the fragments labeled a and b migrated as a doublet of ~3 to 3.5 kb, both containing MVM nt 2199 to 2228, while only the fragment labeled a contained nt 1985 to 2014 and must accordingly represent contiguous sequences from the right end of

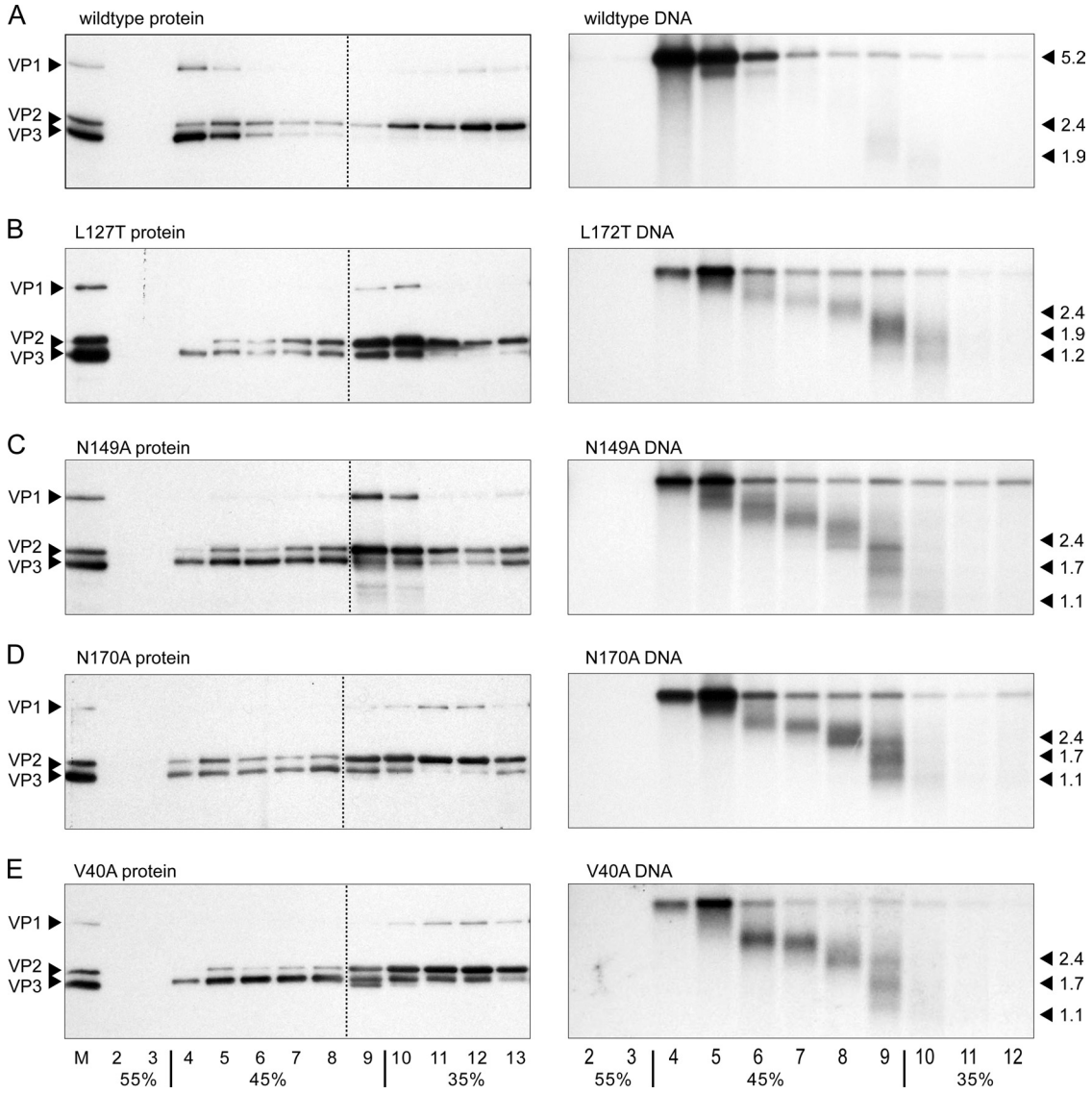

FIG 2 Gradient profiles of viruses generated in multiple-round infections. Iodixanol gradient analyses of wild-type and mutant virus stocks, as indicated, grown at 32°C through multiple cycles in A9 cells are shown. The left side of each pair of panels shows the distribution of capsid proteins in gradient fractions detected by Western transfer using the "allo-p" antipeptide antibody described in Materials and Methods. Lane 1 in each of these blots contained a 50-ng capsid protein standard. Iodixanol percentages in the original step gradient are indicated at the bottom of the figure, and the vertical dotted line between fractions 8 and 9 indicates a loading transition, with lanes representing fractions 2 to 8 each receiving 4-fold more sample than those representing fractions 9 to 13. The right side of each pair of panels shows nuclease-protected viral DNA associated with each fraction, detected following electrophoresis of equal aliquots of each sample through denaturing gels, Southern transfer, and hybridization with a full-length MVMp genomic probe. Positions of MVM restriction fragments used as molecular size markers are indicated, in kilobase pairs, on the right side of each blot.

the genome. Neither of these probes recognized the ~2.3 to 2.4-kb band labeled c, but the top component of this band reacted with a probe at nt 2872 to 2897, while the entire band was seen with the right-end probe (nt 4850 to 4874). Thus, the majority of subgenomic DNAs in fractions 5 to 8 mapped to the 5′ end of the packaged strand, with specific size classes predominating. This banding pattern appears to be a hallmark of the cation-linked uncoating reaction, although at present it is not clear why the mechanism shows a tendency to pause or terminate at specific positions along the genome. The accumulation of such forms in extracts from multiple-round infections of MVM cylinder mutants suggests that compromised interactions between amino acids that make up the base of the 5-fold cylinder result in the intracellular accumulation of large numbers of partially uncoated virions.

While all of the mutants showed approximately similar banding patterns, the differential accumulation of right-end versus left-end sequences was less pronounced in the L172T mutant, where the characteristic pattern of long partially uncoated right-end fragments was accompanied by a comparable smear of long protected sequences that mapped to the 3′ end of the packaged strand, as shown in Fig. 3B. This suggests that the integrity of the L172T genome was compromised in more than one way. Since the cylinders have been implicated as the route of genome entry (25), some

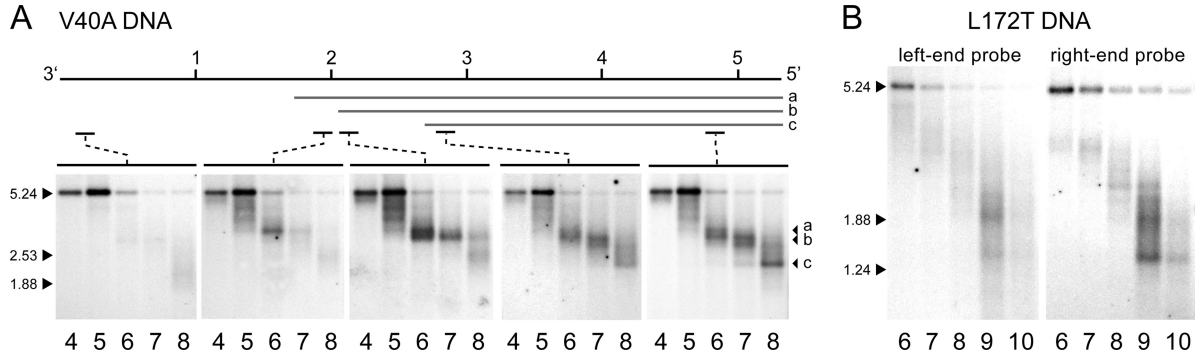

FIG 3 Mapping the origin of subgenomic DNA found in multiple-round infections. (A) Samples from fractions 4 to 8 of the V40A gradient shown in Fig. 2E were digested with micrococcal nuclease and separated by electrophoresis though denaturing gels. Southern transfers after hybridization with ^{32}P-labeled oligonucleotide probes specific for the negative strand at the positions indicated on a linear depiction of the MVM genome are shown. The positions of major bands between ~3.5 and 2.3 kb, labeled a, b, and c, are diagrammed at the top. (B) Southern blots of fractions 6 to 10 from the L172T gradient in Fig. 2B, probed with the left-end or right-end probes shown in panel A.

of this DNA might be due to incomplete packaging or represent previously packaged DNA that was "backing out" of the compromised cylinder in a reversal of the packaging process, that is, in the 5′-to-3′ direction. We conclude that genome integrity in the L172T mutant is compromised by multiple deficits in cylinder function, whereas V40A is vulnerable only to 3′-to-5′ genome uncoating.

We have previously observed that in gradients containing wild-type samples, small amounts of subgenomic DNA typically found in fractions 9 and 10 predominantly comprise defective forms, many of which contain sequences from both ends of the genome but have large internal deletions, as described in detail elsewhere (9, 14). Some fragments seen in fractions 9 and 10 of mutant gradients also hybridized with sequences from both ends of the genome, as shown for L172T in Fig. 3B. However, the sizes of other fragments, relative to the probe positions, indicate that they were derived solely from one end or other of the genome, suggesting that many of these fragments also resulted from the defects in capsid function discussed above.

Initiation of infection is impaired and temperature sensitive for all mutants. To determine whether the N149A, N170A, and V40A mutants exhibit a cell entry defect, as described previously for L172T (11), we tested virions in fraction 5 of each gradient from Fig. 2 for their ability of to initiate a single cycle of infection in A9 cells at input multiplicities of 5,000 or 50,000 genomes per cell (Fig. 4A and B) when cultured at 32°C or 37°C. While the wild-type virus showed high levels of NS1 expression at either of the two temperatures and input multiplicities, its initiation efficiency was invariably higher at 37°C than at 32°C, giving 32°C/37°C initiation ratios of 0.7 to 0.8 (Fig. 4A and B). In contrast, all mutant virions showed impaired initiation at 37°C relative to the wild type, and this reduced initiation was also apparent at 32°C for infections at 5,000 genomes/cell, while at the higher multiplicity most mutants, with the exception of L172T, approached the same high plateau levels. Accordingly, at both input multiplicities each mutant showed impaired infectivity at 37°C compared to 32°C, although L172T was by far the most profoundly affected, with 32°C/37°C ratios of 15 and 7 at 5,000 and 50,000 genomes/cell, respectively, whereas these ratios varied between 2 and 5 for the other mutants. Overall, these observations suggest that all of the mutant virions exhibit an entry defect relative to the wild type that is substantially alleviated at reduced temperature but that L172T is the most temperature sensitive and the most severely impaired.

Effects of VP2-to-VP3 cleavage on VP1 exposure and virion infectivity. We next asked if these mutant virions were able to protect critical VP1 entry domains following extensive VP2-to-VP3 cleavage. For this experiment, full virions from fraction 5 of the wild-type and mutant preparative gradients from Fig. 2 were incubated alone (Fig. 4C to G, lanes 1) or digested with trypsin at 37°C or room temperature (lanes 2 and 3, respectively) for 30 min. Western blots were probed with a mixture of two anti-VP antibodies, which ensures that the minor species, VP1, can be readily visualized, although it does distort the apparent stoichiometry of the viral polypeptides. In each case, almost all of the VP2 forms were cleaved, but the more extreme proteolysis seen at 37°C also led to partial cleavage of VP1 in the mutant samples. We also observed VP1 depletion in these mutants at room temperature after longer digestion periods (not shown), so this cleavage relies not on elevated temperature but simply on more exhaustive proteolysis than is required for VP2 cleavage. Thus, as found previously for L172T (11), the ability of the N149A, N170A, and V40A mutants to protect their VP1 N termini is compromised following removal of the VP2 N termini, suggesting an important role for the latter in stabilizing the mutant 5-fold cylinders.

Aliquots of the samples shown in Fig. 4C to G were then tested for their ability to initiate infection, as assessed by NS1 expression (Fig. 4H), and in each case mutant viral infectivity was almost totally compromised by prior VP2 digestion, even when there was no concomitant *in vitro* cleavage of VP1. We conclude that, in contrast to the case for the wild type, externalized VP2 N termini are essential for the stability of all of the cylinder mutants examined here and that if these peptides are removed before virions encounter the host cell, virus entry is compromised. Since proteolysis during the early stages of entry would likely be minimized at lower temperatures, this vulnerability may in part explain the temperature-sensitive nature of the entry route. However, since all of the mutants exhibited this defect, it is unlikely to fully account for the extreme temperature sensitivity of L172T.

L172T uncoats *in vitro* following proteolysis at 37°C. We have previously shown that L172T undergoes a conformational shift after proteolysis at 37°C, which leaves the genome sensitive to nuclease digestion (11), but this type of treatment would not be

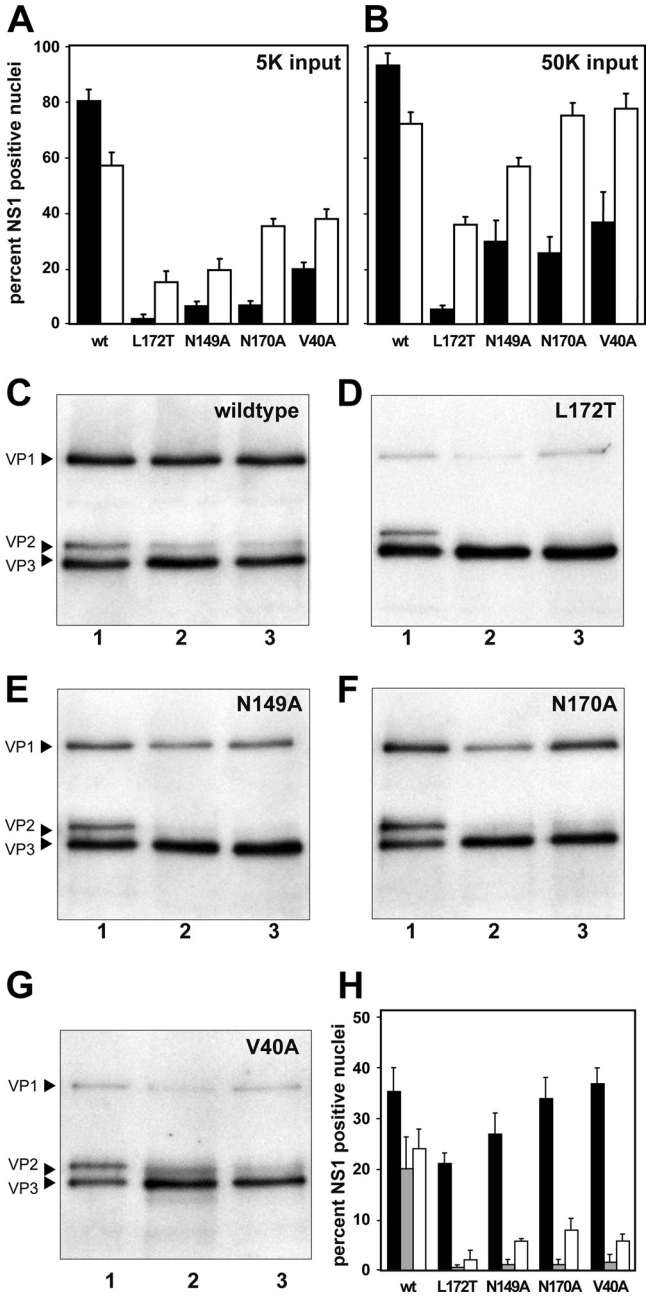

FIG 4 Ability of viruses to initiate infection before and after proteolysis. (A and B) Ability of wild-type and mutant viruses to initiate infection in A9 cells, as measured by the percentage of cells that express NS1. Cells were infected at 5,000 (A) or 50,000 (B) genomes/cell and cultured at 37°C (black bars) or 32°C (white bars). Experiments were performed in duplicate, with each data point representing between 500 and 1,000 cells. (C through G) Western blots of wild-type virions (C) and virions of mutant L172T (D), N149A (E), N170A (F), or V40A (G), either before trypsin digestion (lane 1) or after digestion at 37°C (lane 2) or room temperature (lane 3). Western blots were developed using a mixture of anti-allo-p-specific and VP1 N terminus-specific antipeptide antibodies, as described in Materials and Methods. (H) Samples from each of these reactions were then tested for their ability to initiate infection, which was quantitated by assessing the percentage of cells expressing NS1 after 26 h. Black bars represent untreated samples, while gray and white bars represent samples subjected to trypsin treatment at 37°C and room temperature, respectively.

predicted to induce 3′-to-5′ uncoating in wild-type virus because it does not include a divalent cation depletion step (7). Thus, we wished to establish exactly what factors promote L172T disruption *in vitro*. Accordingly, purified fraction 5 wild-type and L172T virions that had been stored at 4°C in iodixanol buffered with PBS containing 1 mM $MgCl_2$ were incubated at 37°C in the presence of trypsin for 1 h and then subjected to analytical iodixanol gradient centrifugation. As expected, wild-type virus rebanded where full virions typically band in these gradients, in fractions 2 to 4 (Fig. 5A). In contrast, approximately 47% of the L172T particles underwent a structural change that caused them to shift to fractions 6 to 8 (Fig. 5B). Notably, incubation with proteases at 30 or 21°C produced much less pronounced shifts in the banding pattern (of 17% and 9%, respectively) (Fig. 5C and D), as did incubation at 37°C without trypsin (11%) (Fig. 5E), indicating that both exposure to 37°C and VP2 cleavage were required to destabilize the L172T virions.

In contrast, cation-linked 3′-to-5′ genome uncoating of wild-type virus *in vitro* requires prior exposure to chelating buffers and is not dependent upon VP2 cleavage (7). This suggests that L172T may undergo a more complex type of reaction, although divalent cations still played a significant role in the overall response, because addition of 5 mM $MgCl_2$ 1 h before the 37°C incubation step substantially suppressed the L172T rearrangement (from 47% to 14%) (Fig. 5F). Overall, the data indicate that L172T cylinders are extremely fragile and lose the ability to retain DNA at 37°C once their stability is challenged by VP2 cleavage. VP2 cleavage *in vivo* would thus be expected to promote exposure of the L172T genome at 37°C but to be much less damaging at lower temperatures, likely contributing to the extreme temperature sensitivity of this mutant.

Nuclease digestion of fractions from the L172T sample shown in Fig. 5B, which had been digested with trypsin at 37°C, largely removed the uncoated DNA migrating in fractions 7 and 8 and revealed some protected subgenomic species of up to ~3.5 kb in length (Fig. 5I). However, this protected DNA hybridized to probes from both ends of the viral genome (Fig. 5J and K), so it likely represents a mixture of both 3′-to-5′ uncoating and reversal of the packaging process, which leads to 5′-to-3′ extrusion, suggesting that the packaging portal of this mutant loses its integrity under these conditions.

In contrast to the case for L172T, when virions from fraction 5 of the V40A or N149A mutant gradients were incubated with trypsin at 37°C for an hour, they showed relatively minor banding shifts of 13 and 11%, respectively (Fig. 6A and C), which were only slightly more pronounced than the shifts seen without proteolysis (Fig. 6B and D). Thus, V40A and N149A capsids would not be predicted to uncoat *in vivo* at 37°C simply in response to VP2 cleavage, which might explain why they are less severely temperature sensitive than L172T.

The mutants uncoat more readily than the wild type in response to divalent cation depletion. DNA could also be exposed in L172T virions very efficiently by divalent cation depletion. In the sample illustrated in Fig. 5G, this was achieved by diluting the virus into a mildly chelating buffer at high pH (TE8.7), followed by incubation at 4°C for 2 days prior to heating at 37°C for an hour in the absence of proteases. Under these conditions, 91% of the L172T virions shifted their banding position in iodixanol gradients, whereas a sample of wild-type virus treated in parallel showed a 54% shift (Fig. 5H), indicating that L172T was substan-

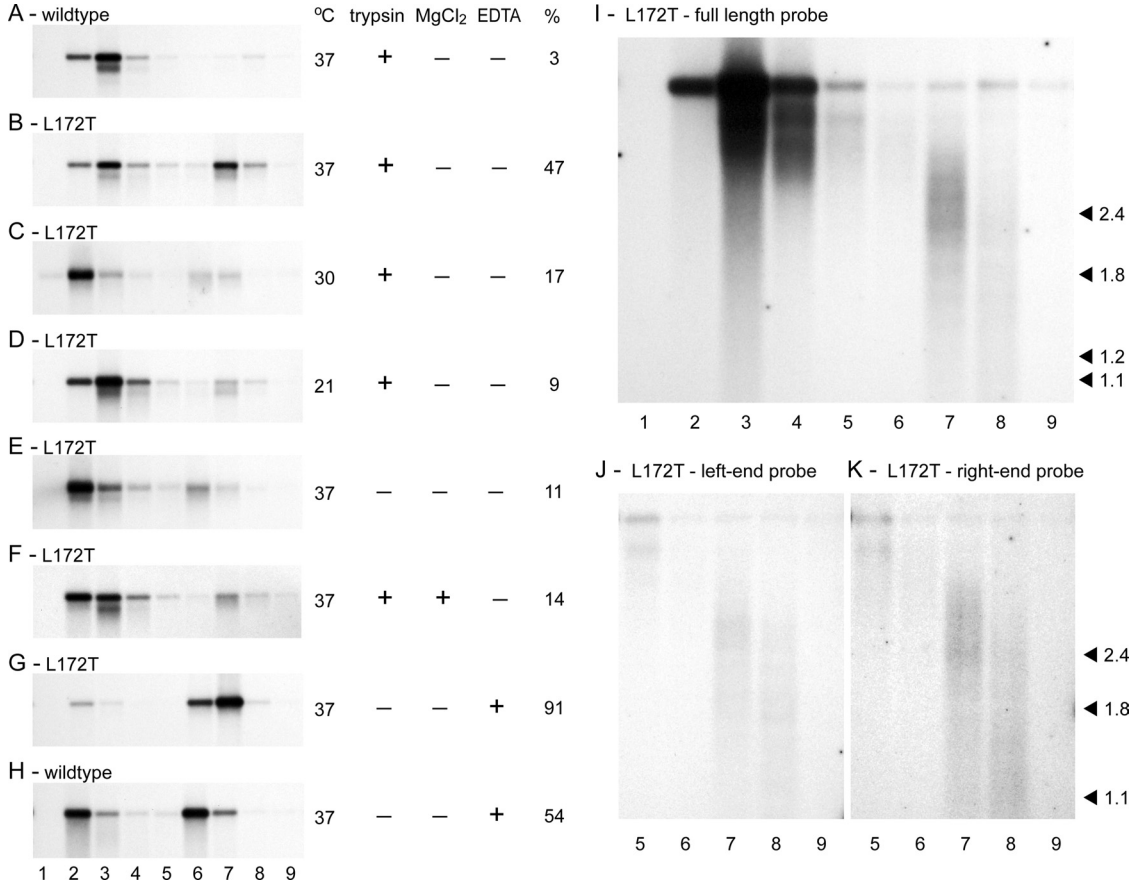

FIG 5 *In vitro* induction of conformational changes that expose L172T DNA. (A through F) Wild-type or L172T mutant virus samples that were incubated with or without trypsin and at various temperatures as shown and then analyzed for evidence of conformational changes by banding through analytical iodixanol gradients. Gradient fractions were subjected to electrophoresis through denaturing gels and analyzed by Southern blotting. Virions that had resisted conformational changes banded in fractions 2 to 4, while uncoated particles banded in fractions 6 to 8. Estimates of the fraction that was uncoated (labeled "%") compare the DNA accumulation in fractions 6 to 8 with the total in fractions 2 to 4 and 6 to 8 combined. (G and H) Samples were treated in a similar way except that these virions were diluted in 3 volumes of TE8.7 buffer and stored at 4°C for 2 days prior to testing. This procedure chelates cations and primes the particles for subsequent heat-induced uncoating. (I through K) Southern transfers of gradient fractions from panel B (i.e., L172T digested with trypsin at 37°C) that were digested with micrococcal nuclease prior to electrophoresis. (I) The Southern blot was hybridized with a random-primed full-length genomic probe. (J and K) Nuclease-treated fractions 5 to 9 from the same gradient, hybridized with a random-primed probe representing either MVM nt 789 to 1043 (left-end probe) (J) or nt 3976 to 4154 (right-end probe) (K).

tially more prone to uncoat than the wild type, even though in this case its VP2 N termini had not been proteolyzed and so were still available to promote cylinder stability. Similarly, all of the other mutants tested showed an enhanced tendency to uncoat compared to wild-type virus when assayed in parallel. Thus, for example, in the assay shown in Fig. 6, after dilution in TE8.7 and incubation for 4 h at 4°C, only ~10% of the wild-type sample shifted (Fig. 6E), whereas 71% of the V40A and 65% of the N149A samples were affected (Fig. 6F and G, respectively). In a separate assay, ~47% of the N170A particles were shifted, compared to 11% for the wild type (data not shown), indicating that this mutant is also compromised in its ability to resist uncoating.

This enhanced tendency for mutants to uncoat following divalent cation depletion was less severe after incubation at 32°C than after incubation at 37°C, but it was still apparent. For example, in an experiment where 23% of the wild-type virus uncoated after incubation at 37°C but only <7% uncoated after incubation at 32°C, 76% of the V40A mutant shifted at 37°C, while 56% still uncoated after incubation at 32°C (not shown). Thus, the impaired infectivity of these mutants may well reflect, in part, an enhanced tendency to uncoat, even at 32°C.

Overall, these assays indicate that all of the mutant viruses are substantially more prone to uncoat following divalent cation depletion than the parental virus. This suggests a role for the 5-fold channel in cation-linked uncoating and raises the possibility that the mutants might be susceptible to premature 3′-to-5′ uncoating *in vivo*, induced by a cellular mechanism during cell entry, which might explain the extensive accumulation of partially uncoated virions seen during multiple-round infections.

In single-round infections there is no evidence of partial encapsidation or extensive uncoating of newly synthesized DNA. Next we assessed the ability of fraction 5 virions from each preparative gradient in Fig. 2 to support viral DNA synthesis in a single-round infection at 37°C (Fig. 7A) or 32°C (Fig. 7B). For this, we infected cells at 10,000 genomes/cell under single-cycle infection conditions and collected both the medium and cells, dividing the cells into two equal aliquots. One half of the cells was used to isolate total intracellular DNA as described in Materials

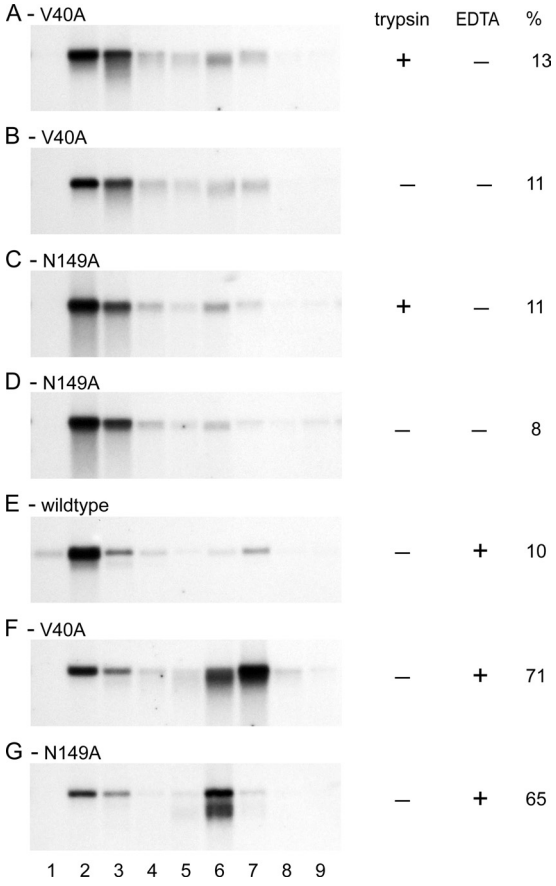

FIG 6 Induction of conformational changes in the V40A and N149A mutants. (A through D) Gradient analyses of V40A or N149A virions following exposure to 37°C, with or without trypsin as shown. Virions were analyzed for evidence of conformational changes by banding through analytical iodixanol gradients. Gradient fractions were subjected to electrophoresis through denaturing gels and analyzed by Southern blotting as described in the legend for Fig. 5. (E through G) Samples that were cation depleted prior to analysis by dilution in 3 volumes of TE8.7 and storage at 4°C for 4 h and analyzed as described above.

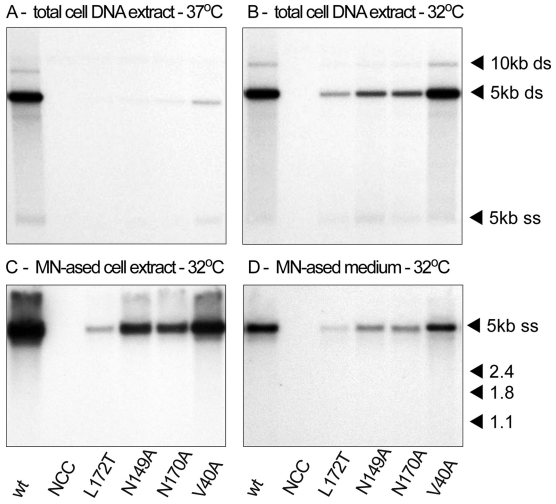

FIG 7 Viral DNA synthesis during single-round infections. (A and B) Total intracellular viral DNA generated in single-round infections at 37°C and 32°C, respectively, analyzed by Southern blotting after electrophoresis through nondenaturing gels. (C) Intracellular virion DNA in a TE8.7 extract of cells cultured at 32°C, following digestion with micrococcal nuclease and electrophoresis through a denaturing gel. (D) Virion DNA in samples of culture medium (containing neuraminidase) from the 32°C incubation, following nuclease digestion and analysis on a denaturing gel.

and Methods, which was analyzed by neutral gel and Southern blotting, as shown in Fig. 7A and B. The other cell aliquot was subjected to freeze-thaw extraction in TE8.7 to generate an extract containing intact viral particles and analyzed for protected DNA, as shown for the 32°C sample in Fig. 7C. As predicted from the previous initiation assays (Fig. 4A and B), we observed very little viral DNA synthesis in mutant virus-infected cells cultured at 37°C, although replication of wild-type virus was robust at this temperature (Fig. 7A). In contrast, duplex replicative-form DNA and progeny single strands were readily apparent for all of the mutants in cells cultured at 32°C (Fig. 7B), and in each case, progeny virions were released into the culture medium (Fig. 7D). Generally, DNA synthesis correlated well with the initiation assays shown in Fig. 4A and B, although V40A replication was exceptionally efficient, approaching wild-type levels at this input multiplicity. These data suggest that the initiation defects seen for each mutant are not further compounded by defects in DNA replication.

Analysis of encapsidated genomes following nuclease digestion in the medium (Fig. 7D) and in TE8.7 extracts (Fig. 7C) from cells cultured at 32°C confirmed that progeny DNAs generated by these mutants were packaged and subsequently released from the cell efficiently and did not contain a significant fraction of subgenomic forms. This suggests that the subgenomic DNAs observed in the multiple-round cultures analyzed in Fig. 2 do not result from defects in DNA synthesis or packaging and, importantly, that such forms were not generated from mutant virions during the process of extraction from the cell. We conclude that viral replication and the generation of progeny virions are normal for these cylinder mutants and that their primary defects precede NS1 expression and likely occur during cell entry.

Cylinder mutants uncoat during cell entry. To explore the latter possibility directly, we infected synchronized (G_0) A9 cells with wild-type or V40A virions at 50,000 genomes/cell in medium containing aphidicolin. This allowed cells to progress to the G_1-S border while virions were trafficked to the cell nucleus, but it prevented transit into S phase. After incubation at 32°C for 24 h, neuraminidase was added to release any noninternalized virus from the cell surface and the cells incubated for a further 4 h before being extracted, as described in Materials and Methods. Significantly, internalized wild-type virus recovered from these cells sedimented predominantly as full-length intact virions, migrating in fractions 3 to 5 (Fig. 8A). In distinct contrast, recovered V40A genomes were predominantly subgenomic and showed multiple discrete forms spread through the gradient from fractions 4 to 9 (Fig. 8B). This pattern closely resembled that of partially uncoated subgenomic DNAs resulting from multiple-round infections shown in Fig. 2, suggesting that, *in vivo*, V40A virions are exceptionally prone to lose their DNA during entry, even at 32°C, in a way that is not seen for the wild type. This possibility is strengthened by the observation that simply adding mutant virus to uninfected cells immediately before lysis did not induce a similar effect, since most of the recovered genomes, shown in Fig. 8C, remained intact and banded in fractions 4 to 6.

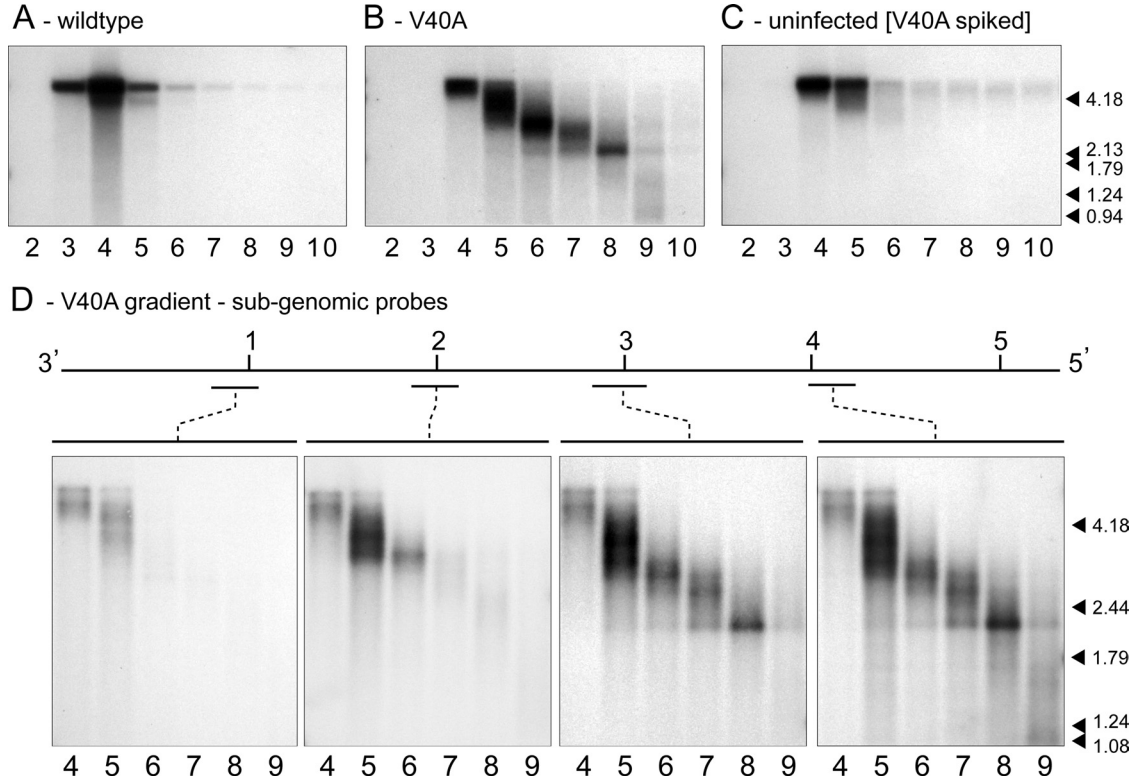

FIG 8 Mutant virions uncoat during cell entry. (A to C) Incoming virion DNA in total cell extracts following fractionation through iodixanol gradients and without *in vitro* nuclease treatment. Before infection cells were synchronized in G_0 by isoleucine deprivation and then infected with wild-type or V40A virions at 32°C (A and B, respectively) or left uninfected (C) in complete medium plus aphidicolin to allow cell cycle progression to the G_1-S border without entry into S phase. Neuraminidase was added at 24 h postinfection to release noninternalized virus, and cells were harvested 4 h later. Prior to cell lysis V40A virus equivalent to 1/10 of the experimental inoculum was added to the uninfected control cells (C), and these were then processed in parallel with test groups. This served as a control for any cleavage or modification that might occur during subsequent extraction and processing. (D) Fractions 4 to 9 of the V40A gradient (from panel B) digested with nuclease prior to electrophoresis and probed with ~200-bp sequences from positions along the MVM genome, as indicated.

To confirm that the subgenomic DNAs seen in fractions 4 to 9 of the V40A infection were the product of 3′-to-5′ uncoating, we digested gradient fractions with micrococcal nuclease and analyzed them following Southern transfer using probes that recognized sequences positioned 1 kb apart along the viral genome (Fig. 8D). A probe that bound 1 kb from the 3′ end of the negative strand recognized predominantly large DNA species of >4 kb in fractions 4 and 5 but very little other material distributed through the gradient. The probe at 2 kb identified these species plus additional strong bands between 3.0 and 3.5 kb, which likely represent contiguous sequences from the right end of the genome and correspond to the species designated a and b in the analysis shown in Fig. 2B. The probe at 3 kb recognized these forms plus an additional ~2.3-kb species that appeared predominantly in fraction 8 (corresponding to the species designated c in Fig. 2B), while the probe at 4 kb recognized all of the above plus additional new lower-molecular-weight bands in fraction 9, which was likely present in the multiple-round infection but could not previously be identified due to accumulation of short DNAs from multiple sources. We conclude that V40A virions have a major cell entry defect in A9 cells, even at 32°C, that is predominantly due to the premature and wholesale induction of 3′-to-5′ uncoating. This strongly implicates the virion cylinder as the route of uncoating and suggests that the V40-L172 side chain interaction is important in regulating this interaction. In contrast, V40A showed no sign of releasing its DNA in a 5′-to-3′ direction, as would be expected following collapse of the packaging portal. Thus, we infer that the V40 interaction does not substantially regulate this gateway, which depends rather upon other features of the L172 residue.

DISCUSSION

In this paper we show that MVMp virions with a variety of cylinder base mutations exhibit cell entry defects that are extreme and debilitating at normal physiological temperatures but can be minimized by growth at 32°C. These defects predominantly involve disruption of the cell entry program built into the virion, which appears to rely upon its metastable properties and which would normally regulate the timely and sequential exposure first of the VP1SR domain and then of the viral genome. Although both of these events can be induced *in vitro* by incremental heating to supraphysiological temperatures (6), the two steps are experimentally separable. Thus, for example, extrusion of VP1 N termini *in vitro* initiates at lower temperatures than are required for genome uncoating, while genome exposure in response to divalent cation depletion occurs efficiently without VP1SR externalization (7). The fact that all of the mutants studied here showed enhanced VP1SR and 3′-to-5′ genome exposure suggests that both of these extrusion events reflect a normal pattern of conformational shifts that are required *in vivo* to mediate infectious entry. In contrast, the L172T mutant also allows release of the genome via its

genomic right-hand end, effectively reversing the packaging direction of the DNA, presumably due to collapse of the packaging portal. The extreme vulnerability of L172T thus appears to reflect the central role of this residue in the stability and dynamics of the cylinder, where the 5-fold-related leucine side chains both define the size and character of the tightest constriction point at the base of the cylinder and also establish specific interactions with V40 from VP N termini that will eventually be everted through this structure (1, 25).

While all of the mutant virions were found to be compromised in their ability to restrain 3′-to-5′ genome uncoating, both *in vitro* following cation depletion and *in vivo* during cell entry, precisely where in the cell these mutant viruses uncoat remains to be determined. Since subsequent nuclease digestion had little, if any, effect on the length of the partially protected mutant DNA, the exposed nucleotides appear to have been resected prior to gradient fractionation. This suggests exposure to a nucleolytic acidic or hydrolase-rich environment, such as might be encountered during entry in an endosomal or lysosomal vacuole. When associated with this type of extensive genome truncation, the widespread uncoating of mutant particles leads to virus inactivation. However, if 3′-to-5′ uncoating does play a critical role during productive infection, it might be expected to occur in a neutral cellular compartment, perhaps following bilayer transit into the cytoplasm at the earliest. Alternatively, since parvoviral virions are small enough to cross the nuclear pore and do appear to be able to penetrate into the nucleus (23, 27, 28, 31) and the VP1SR contains functional nuclear localization signals (22), uncoating probably occurs in the nucleus. Trafficking studies indicate that relatively few incoming parvovirus particles ever reach the cytosol or nucleus (23, 28), suggesting that during the course of a normal infection, only a small fraction of the cell-associated wild-type virus might extrude its DNA by this mechanism, presumably at a specific location and in response to a specific cellular trigger.

A second significant finding from the present study is that none of the mutants were able to protect their VP1SR domains from proteolysis following extensive cleavage of externalized VP2 N termini, as previously reported for L172T (11). This suggests that the exposed VP2 peptides stabilize the mutant cylinders and that, by analogy, they may serve a similar role in wild-type virus. In support of this idea, we have previously shown that proteolysis of VP2 N termini lowers the energy required to induce VP1SR exposure *in vitro* (6). One possible mechanism for VP2-mediated stabilization could involve the glycine-rich sequences that are threaded through the cylinder. If these are effectively tethered at the particle surface, perhaps by the bulky side chains of the externalized peptide, they could hold the cylinder under tension, but when the N termini are cleaved and the tension released, the walls of the cylinder could lose cohesion and start to open. VP2 cleavage thus appears to resemble the activation cleavage steps seen for members of other nonenveloped virus families, where an apparently stable virion sustains a specific proteolytic clip that facilitates subsequent exposure of a peptide known to be essential for membrane penetration (3, 5). This strategy allows the particle to exist transiently in a metastable state, where the lowest-energy form of the cleaved product is initially shielded by the energy barrier between the two forms (18). During entry, such viruses typically encounter some form of catalyst, which releases the metastable configuration of the cleaved structure, allowing *de novo* exposure of a sequence, such as the MVM VP1SR PLA_2 domain (33), that is required for bilayer penetration (13). However, what the releasing catalyst is for MVM and its vacuolar location remain unknown.

When expressed as VP2-only VLPs, the V40A, N149A, and N170A mutants studied here (together with mutants carrying alanine mutations at VP2 S43, N263, and F526) all failed to show a tryptophan fluorescence inflection at ~46°C that is normally seen in wild-type VLPs and presumably reflects a sharp heat-induced conformational rearrangement (26). Induction of this fluorescence shift also appeared to correlate with the externalization of VP2 N termini as measured by a transient heating and proteolysis assay (17). These observations suggested that the mutations might impose increased rigidity on the cylinder that prevents extrusion of their VP N termini, as shown for adeno-associated virus type 2 (AAV2) (2) (discussed below). However, our studies suggest an alternative interpretation, namely, that the fluorescence shift reflects release of a structural constraint that is able to keep wild-type cylinders in a metastable state at physiological temperatures but which is missing in the mutants, so that the latter are effectively in the open configuration. This type of defect might well render mutant virions incapable of retaining their VP1SR, as reported here, once the restraint imposed by their externalized VP2 N termini is removed.

For the related parvovirus AAV2, a member of the genus *Dependovirus*, VP1 residue L336 occupies a position equivalent to VP2 L172 in MVM. Mutations at this site in AAV2 lead not to cylinder collapse but rather to the inability of the cylinder to open and allow egress of VP N termini (2). While the 5-fold cylinders of all the vertebrate parvoviruses are substantially conserved, differences in coding strategy between MVM and AAV mean that it is possible that the 5-fold cylinders of AAV would need to open only once to allow the emergence of all 10 of their VP1 and VP2 N termini. However, in MVM the cylinders are apparently required to open and close reversibly and repeatedly, to allow the exposure of up to 50 VP2 N termini, before opening in an apparently irreversible manner to allow egress of the VP1SR (6, 30). Why members of the genus *Parvovirus* have evolved such a complex mechanism is unclear, but it likely reflects significant differences in the lifestyles of the two genera.

ACKNOWLEDGMENTS

We thank Mauricio G. Mateu for kindly providing MVM plasmids encoding the N149A, N170A, and V40A mutations.

This work was supported by Public Health Service grants CA029303 and AI026109 from the National Institutes of Health.

REFERENCES

1. **Agbandje-McKenna M, Llamas-Saiz AL, Wang F, Tattersall P, Rossmann MG.** 1998. Functional implications of the structure of the murine parvovirus, minute virus of mice. Structure **6**:1369–1381.
2. **Bleker S, Sonntag F, Kleinschmidt JA.** 2005. Mutational analysis of narrow pores at the fivefold symmetry axes of adeno-associated virus type 2 capsids reveals a dual role in genome packaging and activation of phospholipase A2 activity. J. Virol. **79**:2528–2540.
3. **Bubeck D, et al.** 2005. The structure of the poliovirus 135S cell entry intermediate at 10-angstrom resolution reveals the location of an externalized polypeptide that binds to membranes. J. Virol. **79**:7745–7755.
4. **Carrasco C, et al.** 2009. The capillarity of nanometric water menisci confined inside closed-geometry viral cages. Proc. Natl. Acad. Sci. U. S. A. **106**:5475–5480.
5. **Chandran K, Parker JS, Ehrlich M, Kirchhausen T, Nibert ML.** 2003. The delta region of outer-capsid protein micro 1 undergoes conforma-

tional change and release from reovirus particles during cell entry. J. Virol. **77**:13361–13375.
6. **Cotmore SF, D'Abramo AM, Ticknor CM, Tattersall P.** 1999. Controlled conformational transitions in the MVM virion expose the VP1 N-terminus and viral genome without particle disassembly. Virology **254**: 169–181.
7. **Cotmore SF, Hafenstein S, Tattersall P.** 2010. Depletion of virion-associated divalent cations induces parvovirus minute virus of mice to eject its genome in a 3′-to-5′ direction from an otherwise intact viral particle. J. Virol. **84**:1945–1956.
8. **Cotmore SF, Tattersall P.** 1987. The autonomously replicating parvoviruses of vertebrates. Adv. Virus Res. **33**:91–174.
9. **Cotmore SF, Tattersall P.** 2005. Encapsidation of minute virus of mice DNA: aspects of the translocation mechanism revealed by the structure of partially packaged genomes. Virology **336**:100–112.
10. **Cotmore SF, Tattersall P.** 2007. Parvoviral host range and cell entry mechanisms. Adv. Virus Res. **70**:183–232.
11. **Farr GA, Cotmore SF, Tattersall P.** 2006. VP2 cleavage and the leucine ring at the base of the fivefold cylinder control pH-dependent externalization of both the VP1 N terminus and the genome of minute virus of mice. J. Virol. **80**:161–171.
12. **Farr GA, Tattersall P.** 2004. A conserved leucine that constricts the pore through the capsid fivefold cylinder plays a central role in parvoviral infection. Virology **323**:243–256.
13. **Farr GA, Zhang LG, Tattersall P.** 2005. Parvoviral virions deploy a capsid-tethered lipolytic enzyme to breach the endosomal membrane during cell entry. Proc. Natl. Acad. Sci. U. S. A. **102**:17148–17153.
14. **Faust EA, Ward DC.** 1979. Incomplete genomes of the parvovirus minute virus of mice: selective conservation of genome termini, including the origin for DNA replication. J. Virol. **32**:276–292.
15. **Gardiner EM, Tattersall P.** 1988. Mapping of the fibrotropic and lymphotropic host range determinants of the parvovirus minute virus of mice. J. Virol. **62**:2605–2613.
16. **Govindasamy L, et al.** 2010. MVM capsid dynamics associated with DNA packaging and VP2 externalization for maturation cleavage, poster P11. XIII International Parvovirus Workshop, Helsinki, Finland.
17. **Hernando E, et al.** 2000. Biochemical and physical characterization of parvovirus minute virus of mice virus-like particles. Virology **267**: 299–309.
18. **Hogle JM.** 2002. Poliovirus cell entry: common structural themes in viral cell entry pathways. Annu. Rev. Microbiol. **56**:677–702.
19. **King JA, Dubielzig R, Grimm D, Kleinschmidt JA.** 2001. DNA helicase-mediated packaging of adeno-associated virus type 2 genomes into preformed capsids. EMBO J. **20**:3282–3291.
20. **Kontou M, et al.** 2005. Structural determinants of tissue tropism and in vivo pathogenicity for the parvovirus minute virus of mice. J. Virol. **79**: 10931–10943.
21. **Llamas-Saiz al, et al.** 1997. Structure determination of minute virus of mice. Acta Crystallogr. D Biol. Crystallogr. **53**:93–102.
22. **Lombardo E, Ramírez JC, Garcia J, Almendral JM.** 2002. Complementary roles of multiple nuclear targeting signals in the capsid proteins of the parvovirus minute virus of mice during assembly and onset of infection. J. Virol. **76**:7049–7059.
23. **Mani B, et al.** 2006. Low pH-dependent endosomal processing of the incoming parvovirus minute virus of mice virion leads to externalization of the VP1 N-terminal sequence (N-VP1), N-VP2 cleavage, and uncoating of the full-length genome. J. Virol. **80**:1015–1024.
24. **Morgan WR, Ward DC.** 1986. Three splicing patterns are used to excise the small intron common to all minute virus of mice RNAs. J. Virol. **60**:1170–1174.
25. **Plevka P, et al.** 2011. Structure of a packaging-defective mutant of minute virus of mice indicates that the genome is packaged via a pore at a 5-fold axis. J. Virol. **85**:4822–4827.
26. **Reguera J, Carreira A, Riolobos L, Almendral JM, Mateu MG.** 2004. Role of interfacial amino acid residues in assembly, stability, and conformation of a spherical virus capsid. Proc. Natl. Acad. Sci. U. S. A. **101**: 2724–2729.
27. **Sonntag F, Bleker S, Leuchs B, Fischer R, Kleinschmidt JA.** 2006. Adeno-associated virus type 2 capsids with externalized VP1/VP2 trafficking domains are generated prior to passage through the cytoplasm and are maintained until uncoating occurs in the nucleus. J. Virol. **80**: 11040–11054.
28. **Suikkanen S, et al.** 2003. Exploitation of microtubule cytoskeleton and dynein during parvoviral traffic toward the nucleus. J. Virol. **77**: 10270–10279.
29. **Tattersall P, Cawte PJ, Shatkin AJ, Ward DC.** 1976. Three structural polypeptides coded for by minute virus of mice, a parvovirus. J. Virol. **20**:273–289.
30. **Tattersall P, Shatkin AJ, Ward DC.** 1977. Sequence homology between the structural polypeptides of minute virus of mice. J. Mol. Biol. **111**: 375–394.
31. **Vihinen-Ranta M, Yuan W, Parrish CR.** 2000. Cytoplasmic trafficking of the canine parvovirus capsid and its role in infection and nuclear transport. J. Virol. **74**:4853–4859.
32. **Yeung DE, et al.** 1991. Monoclonal antibodies to the major nonstructural nuclear protein of minute virus of mice. Virology **181**:35–45.
33. **Zadori Z, et al.** 2001. A viral phospholipase A2 is required for parvovirus infectivity. Dev. Cell **1**:291–302.